doi:10.1093/brain/awu344 BRAIN 2015: 138; 549–562 | 549

BRAIN
A JOURNAL OF NEUROLOGY

In vivo detection of nerve injury in familial amyloid polyneuropathy by magnetic resonance neurography

Jennifer Kollmer,[1,2] Ernst Hund,[2,3] Benjamin Hornung,[1] Ute Hegenbart,[2,4] Stefan O. Schönland,[2,4] Christoph Kimmich,[2,4] Arnt V. Kristen,[2,5] Jan Purrucker,[2,3] Christoph Röcken,[6] Sabine Heiland,[1,7] Martin Bendszus[1] and Mirko Pham[1,2]

See Morrow and Reilly (doi:10.1093/awu396) for a scientific commentary on this article.

Transthyretin familial amyloid polyneuropathy is a rare, autosomal-dominant inherited multisystem disorder usually manifesting with a rapidly progressive, axonal, distally-symmetric polyneuropathy. The detection of nerve injury by nerve conduction studies is limited, due to preferential involvement of small-fibres in early stages. We investigated whether lower limb nerve-injury can be detected, localized and quantified *in vivo* by high-resolution magnetic resonance neurography. We prospectively included 20 patients (12 male and eight female patients, mean age 47.9 years, range 26–66) with confirmed mutation in the transthyretin gene: 13 with symptomatic polyneuropathy and seven asymptomatic gene carriers. A large age- and sex-matched cohort of healthy volunteers served as controls (20 male and 20 female, mean age 48.1 years, range 30–73). All patients received detailed neurological and electrophysiological examinations and were scored using the Neuropathy Impairment Score–Lower Limbs, Neuropathy Deficit and Neuropathy Symptom Score. Magnetic resonance neurography (3 T) was performed with large longitudinal coverage from proximal thigh to ankle-level and separately for each leg (140 axial slices/leg) by using axial T_2-weighted (repetition time/echo time = 5970/55 ms) and dual echo (repetition time 5210 ms, echo times 12 and 73 ms) turbo spin echo 2D sequences with spectral fat saturation. A 3D T_2-weighted inversion-recovery sequence (repetition time/echo time 3000/202 ms) was acquired for imaging of the spinal nerves and lumbar plexus (50 axial slice reformations). Precise manual segmentation of the spinal/sciatic/tibial/common peroneal nerves was performed on each slice. Histogram-based normalization of nerve–voxel signal intensities was performed using the age- and sex-matched control group as normative reference. Nerve-voxels were subsequently classified as lesion-voxels if a threshold of >1.2 (normalized signal-intensity) was exceeded. At distal thigh level, where a predominant nerve–lesion–voxel burden was observed, signal quantification was performed by calculating proton spin density and T_2-relaxation time as microstructural markers of nerve tissue integrity. The total number of nerve–lesion voxels (cumulated from proximal-to-distal) was significantly higher in symptomatic patients (20 405 $\pm$ 1586) versus asymptomatic gene carriers (12 294 $\pm$ 3199; $P = 0.036$) and versus controls (6536 $\pm$ 467; $P < 0.0001$). It was also higher in asymptomatic carriers compared to controls ($P = 0.043$). The number of nerve–lesion voxels was significantly higher at thigh level compared to more distal levels (lower leg/ankle) of the lower extremities (f-value = 279.22, $P < 0.0001$). Further signal-quantification at this proximal site (thigh level) revealed a significant increase of proton-density ($P < 0.0001$) and T_2-relaxation-time ($P = 0.0011$) in symptomatic patients, whereas asymptomatic gene-carriers presented with a significant increase of proton-density only. Lower limb nerve injury could be detected and quantified *in vivo* on microstructural level by magnetic resonance neurography in symptomatic familial amyloid polyneuropathy, and also in yet asymptomatic gene carriers, in whom imaging detection precedes clinical and electrophysiological manifestation. Although symptoms start and prevail distally, the focus of predominant nerve injury and injury progression was found proximally at thigh level with strong and unambiguous lesion-contrast. Imaging of proximal nerve lesions, which are difficult to detect by nerve conduction studies, may have future implications also for other distally-symmetric polyneuropathies.

1 Department of Neuroradiology, University of Heidelberg, Heidelberg, Germany
2 Amyloidosis Centre Heidelberg, University of Heidelberg, Heidelberg, Germany

Received May 27, 2014. Revised September 29, 2014. Accepted October 26, 2014. Advance Access publication December 19, 2014

3 Department of Neurology, University of Heidelberg, Heidelberg, Germany
4 Medical Department V, University of Heidelberg, Heidelberg, Germany
5 Medical Department III, University of Heidelberg, Heidelberg, Germany
6 Department of Pathology, University Hospital Kiel, Kiel, Germany
7 Division of Experimental Radiology, Department of Neuroradiology, University of Heidelberg, Heidelberg, Germany

Correspondence to: Dr Jennifer Kollmer,
Department of Neuroradiology,
University of Heidelberg,
Im Neuenheimer Feld 400,
69120 Heidelberg,
Germany
E-mail: jennifer.kollmer@med.uni-heidelberg.de

Keywords: transthyretin familial amyloid polyneuropathy; amyloid polyneuropathy; MR neurography; MR imaging; hereditary amyloidosis

Abbreviations: FAP = familial amyloid polyneuropathy; MR = magnetic resonance; T_{2app} = apparent T_2 relaxation time

Introduction

Transthyretin (*TTR*) familial amyloid polyneuropathy (FAP) is a fatal multisystem disorder with autosomal-dominant inheritance, leading to misfolding and extracellular deposition of the protein TTR. Encoded on chromosome 18, TTR is a physiological transporter of serum thyroxine and retinol binding protein (Benson, 1989; Buxbaum and Tagoe, 2000). Until now, >120 causative point mutations have been described, with substitution of valine by methionine at position 30 (Val30Met) being the most frequent (Buxbaum and Tagoe, 2000; Hund *et al.*, 2001; Reilly, 2005). With an estimated incidence of ~1 in 1 000 000, TTR-FAP is very rare in the USA (Benson, 1995), but endemic foci are known to occur, e.g. in Portugal, where it was first described by Andrade (1952), and also in Sweden and Japan. TTR-FAP usually manifests with a rapidly progressive and incapacitating distally symmetric sensorymotor polyneuropathy, cardiac and autonomic dysfunction and leads to death at an average of 10 years after onset of symptoms (Plante-Bordeneuve *et al.*, 1998; Hund *et al.*, 2001). Early symptoms of TTR-FAP typically occur symmetrically in the distal lower extremities with tingling and prickly burning sensations of pain, indicating early injury of small nerve fibres (Thomas and King, 1974; Said *et al.*, 1984; Plante-Bordeneuve and Said, 2011). With disease progression and involvement of large-myelinated fibres, manifest sensorimotor polyneuropathy evolves (Van Allen *et al.*, 1969; Reilly, 2005). As mutant TTR is produced mainly in the liver, orthotopic liver transplantation has been the only causative therapy for a long time (Holmgren *et al.*, 1993; Bergethon *et al.*, 1996; Adams *et al.*, 2000). Recently, tafamidis meglumine (Vyndaqel®, Pfizer Inc.), which acts as kinetic stabilizer of the TTR-tetramer has been approved. First clinical results have shown a beneficial effect on disease progression, but regression of amyloid deposition or reversal of structural nerve injury seems to be unlikely (Coelho *et al.*, 2012; Johnson *et al.*, 2012). Similar promising results have been reported for the non-steroidal anti-inflammatory agent diflunisal (Dolobid®; Merck&Co. Inc) (Berk *et al.*, 2013).

As nerve conduction studies are able to measure dysfunction of large myelinated fibres, but not of small or unmyelinated fibres, the early detection of TTR-FAP remains difficult. Moreover, nerve conduction studies are limited in determining the spatial extension of nerve injury, pathomorphological alteration and, to some degree, these methods are also limited in precise lesion localization, in particular in the proximal lower extremities (Said and Plante-Bordeneuve, 2012). Nerve biopsy can show endoneurial amyloid deposits and small-fibre reduction in TTR-FAP (Reilly, 2005; Plante-Bordeneuve and Said, 2011), but is restricted mainly to sural nerve or skin biopsies providing limited tissue specimens that may not necessarily be representative of the underlying disease and mechanisms of injury (Hanyu *et al.*, 1989; Simmons *et al.*, 1993). High-resolution magnetic resonance (MR) neurography has been proven to detect and localize nerve injury on the level of individual nerve fascicles in various experimental and human non-focal metabolic, inflammatory and also focal neuropathies (Filler *et al.*, 1993; Bendszus and Stoll, 2005; Stoll and Bendszus, 2009; Stoll *et al.*, 2009; Kollmer *et al.*, 2012; Pham *et al.*, 2014). MR-neurography has not been investigated in TTR-FAP so far. With an extensive MR-neurography imaging protocol providing both, high spatial resolution and large anatomical coverage, we investigated 20 rare patients with either symptomatic TTR-FAP or asymptomatic gene carriers and a large population of age- and sex-matched healthy controls. The *in vivo* detection, localization and quantification of nerve injury in TTR-FAP by imaging might improve early diagnosis and initiation of causative treatment. It may also suggest novel biomarkers for early monitoring of microstructural nerve injury, which would aid in testing and developing future strategies of pharmacological intervention. Finally, imaging data about nerve lesion sites, lesion extension, and about whether there is an underlying diffuse or non-diffuse pattern of injury would be valuable, because the spatial information about lesion dispersion from nerve conduction studies is limited.

Materials and methods

Study design, clinical and electrophysiological examination

Twenty patients, each with a confirmed mutation in the *TTR* gene (12 male, eight female, mean age 47.9 years, range 26–66), and 40 healthy volunteers matched for gender and age (20 male, 20 female, mean age 48.1 years, range 30–73) were included in this prospective, single-centre study between March 2011 and November 2012. Inclusion criteria were age 18 to 75 years, and for patients, a documented mutation in the *TTR* gene. Only such mutations were included (Val30Met, Leu58His, Tyr69His, Glu54Gly, Phe64Val, Ile107Val, Leu78His, Thr60Ala, Glu54Gln) that are known to be closely associated with a clinical phenotype of a predominant involvement of the peripheral nervous system (Table 1). Patients with prior liver transplantation or prior treatment with disease modifying drugs, such as tafamidis meglumine were excluded. Diabetes mellitus, alcoholism, any malignant or infectious illness as risk factors for polyneuropathy or presence of any contraindications for MRI were further exclusion criteria. By detailed interrogation, any episodes of acute or chronic pain, any sensory or motor symptoms in the upper or lower extremities and any history of (poly)neuropathy were ruled out in all healthy volunteers. The study was approved by the institutional ethics board (University of Heidelberg; S-057/2009) and all participants gave written informed consent before participation.

A detailed neurological examination was performed and past medical history obtained in all patients by a single examiner (E.H., board-certified neurologist with 15 years of experience in clinical neurophysiology, and diagnosis and treatment of TTR-FAP). Physical parameters included sensory and motor function with the following modalities tested in each patient: touch pressure, pinprick sensation, thermal sensibility, vibration perception in both feet, quadriceps and ankle reflexes. Lower limb muscle strengths were graded according to the Medical Research Council (MRC) scale, observing hip, knee, toe extension and flexion, as well as ankle dorsiflexion and plantar flexion. Peripheral neuropathy was scored and classified in all patients according to the following established scales: (i) Neuropathy Impairment Score in the Lower Limbs; (ii) Neuropathy Symptom Score; and (iii) Neurologic Disability Score (Neuropathy Deficit Score) (Dyck, 1988; Dyck *et al.*, 1997; Bril, 1999). Detailed nerve conduction studies were performed in all participants by the same examiner (E.H.) and included measurements of distal motor latency of the peroneal and tibial nerve, nerve conduction velocity in the peroneal, tibial and sural nerve, sensory nerve action potentials of the sural nerve and compound muscle action potential of the

Table 1 Summary of individual mutations, clinical features and scoring in asymptomatic gene carriers and symptomatic TTR-FAP

Case	Age/Sex	Mutation	Age at Onset	Familiarity for neuropathy	Symptoms at onset	Associated clinical features	Amyloid in sural nerve	NSS	NDS	NIS-LL
Asymptomatic gene carriers										
1	33/F	Val30Met	Asymptomatic	Yes	N/A	N/A	Not performed	0	0	0
2	35/F	Val30Met	Asymptomatic	Yes	N/A	N/A	Not performed	0	0	0
3	26/F	Leu58His	Asymptomatic	Yes	N/A	N/A	Not performed	0	0	0
4	33/F	Leu58His	Asymptomatic	Yes	N/A	N/A	Not performed	0	0	0
5	55/M	Val30Met	Asymptomatic	Yes	N/A	N/A	Not performed	0	0	0
6	66/M	Val30Met	Asymptomatic	Yes	N/A	N/A	Not performed	0	0	0
7	52/M	Tyr69His	Asymptomatic	No	Aphasia	Meningeal amyloidosis	Not performed	0	0	0
Symptomatic TTR-FAP										
8	57/M	Val30Met	54	No	Lower limb painful paraesthesia	Gastrointestinal	Not performed	5	10	14
9	49/M	Val30Met	46	Yes	Upper and lower limb paraesthesia	No	Yes	6	10	19
10	35/F	Glu54Gly	31	Yes	Lower limb paraesthesia	Cardial	Yes	5	8	34
11	37/F	Phe64Val	34	Yes	Lower limb paraesthesia	Gastrointestinal Autonomic Cardial	Yes	5	10	42
12	46/F	Val30Met	42	Yes	Lower limb paraesthesia	Gastrointestinal Autonomic cardial	Not performed	5	10	48.5
13	26/F	Val30Met	25	Yes	Lower limb paraesthesia	No	Not performed	6	8	6
14	58/M	Ile107Val	49	No	Bilateral CTS	Cardial	No	6	10	36
15	59/M	Val30Met	56	Yes	Lower limb painful paraesthesia	Gastrointestinal Cardial	No	6	8	8
16	62/M	Val30Met	57	No		Cardial CTS	No	6	10	14
17	59/M	Val30Met	55	Yes	Lower limb paraesthesia	Cardial	No	5	10	12
18	58/M	Leu78His	51	Yes	Bilateral CTS	CTS	Yes	5	10	62
19	64/M	Thr60Ala	61	Yes	Lower limb paraesthesia	Cardial CTS	Yes	5	10	48.5
20	48/M	Glu54Gln	46	No	Lower limb paraesthesia	Cardial CTS	Yes	5	2	22

CTS = carpal tunnel syndrome; NDS = Neuropathy Deficit Score; NIS-LL = Neuropathy Impairment Score in the Lower Limbs; NSS = Neuropathy Symptom Score.

peroneal and tibial nerve. Additionally, the sympathetic skin response was evaluated to detect autonomic dysfunction (Shahani *et al.*, 1984; Shivji and Ashby, 1999; Said and Plante-Bordeneuve, 2012). Concomitant causes of neuropathic injury and symptoms were rendered unlikely by applying strict diagnostic criteria for determining TTR-FAP and by the following serum and urine markers to further rule out other polyneuropathies like diabetic polyneuropathy, alcohol-related polyneuropathy or systemic light-chain amyloidosis: haemoglobin A1c, fasting plasma glucose, vitamin B12 levels, complete blood cell count, complete metabolic panel (including electrolytes, liver and renal panel), thyroid function tests, Bence-Jones proteinuria, serum-free light-chains, immunofixation in serum and urine. Furthermore, all symptomatic and asymptomatic subjects were evaluated extensively for other organ manifestations by board-certified clinicians, experienced in diagnosing and treating all forms of amyloidosis in the interdisciplinary Amyloidosis Centre (U.H., S.S., C.K. and A.K.).

According to clinical and electrophysiological findings all patients were then classified into either symptomatic patients or asymptomatic carriers of any mutation in the *TTR* gene. Asymptomatic status was determined if gene carriers scored '0' in all three clinical polyneuropathy scores (Neuropathy Impairment Score–lower limbs, Neuropathy Deficit Score, Neuropathy Symptom Score). In addition, to be classified as asymptomatic, a normal electrophysiological examination was required with a maximum of one aberrant parameter allowed (Table 2).

According to these criteria, seven participants were classified as asymptomatic gene carriers (three male, four female, mean age 42.9 years, range 26–66) and 13 as patients with symptomatic TTR-FAP (nine male, four female, mean age 50.6 years, range 26–64). All patients in the latter group were affected with a symptom severity score of at least '1' in each of the evaluated clinical polyneuropathy score (Neuropathy Symptom Score/Neuropathy Impairment Score–lower limbs/Neuropathy Deficit Score), and all presented pathological electrophysiological results in more than one of the evaluated parameters.

Histology and immunohistochemistry

Amyloid in sural nerve specimens (available in 8 of 13 symptomatic TTR-FAP patients) was detected by Congo red staining viewed under polarized light showing green birefringence and Congo red fluorescence. Immunohistochemical classification was carried out as described in detail elsewhere (Kebbel and Rocken, 2006; Yumlu *et al.*, 2009; Schonland *et al.*, 2012; Gioeva *et al.*, 2013) with commercially available monoclonal antibodies directed against AA-amyloid, and polyclonal antibodies directed against amyloid P-component, λ-light chain, κ-light chain, fibrinogen; all from Dako. In addition, we used non-commercially available polyclonal antibodies directed against apolipoprotein AI (anti-apoAI), transthyretin (ATTR3) and λ-light chain-derived amyloid proteins (AL1), and anti-λ-light chain-peptide antibodies (AL3 and AL7), and anti-κ-light chain (AK3) (Kebbel and Rocken, 2006; Schonland *et al.*, 2012; Gioeva *et al.*, 2013).

Table 2 Summary of electrophysiological studies in asymptomatic gene carriers and symptomatic TTR-FAP

Case	Age/Sex	Mutation	SSR palmar	SSR plantar	Peroneal nerve			Tibial nerve			Sural nerve	
					NCV	DML	CMAP	NCV	DML	CMAP	NCV	SNAP
Asymptomatic gene carriers												
01	33/F	Val30Met	Normal	Normal	Normal	Normal	Normal	Normal	Normal	Normal	Normal	Normal
02	35/F	Val30Met	Normal	Normal	50 m/s	4.9 ms	12.0 mV	46.8 m/s	4.2 ms	16 mV	43.1 m/s	14 μV
03	26/F	Leu58His	Normal	Normal	51 m/s	4.5 ms	8.0 mV	52 m/s	3.7 ms	14.5 mV	44.8 m/s	5.3 μV
04	33/F	Leu58His	Normal	Normal	49 m/s	2.91 ms	8.0 mV	51 m/s	3.6 ms	21.5 mV	51 m/s	8.9 μV
05	55/M	Val30Met	Normal	Normal	Normal	Normal	Normal	Normal	Normal	Normal	Normal	Normal
06	66/M	Val30Met	Normal	Normal	Normal	Normal	Normal	Normal	Normal	Normal	Normal	Normal
07	52/M	Tyr69His	Normal	Normal	N/A	N/A	N/A	45 m/s	4.3 ms	5.2 mV	55 m/s	6.5 μV
Symptomatic TTR-FAP												
08	57/M	Val30Met	Normal	Absent	36 m/s	9.8 ms	0.74 mV	34 m/s	7.0 ms	0.88 mV	Absent	Absent
09	49/M	Val30Met	Normal	Normal	36 m/s	5.83 ms	0.76 mV	41 m/s	4.17 ms	3.3 mV	Absent	Absent
10	35/F	Glu54Gly	Absent	Absent	Absent	Absent	Absent	Absent	Absent	Absent	Absent	Absent
11	37/F	Phe64Val	Absent	Absent	Absent	Absent	Absent	34.3 m/s	5.2 ms	0.41 mV	Absent	Absent
12	46/F	Val30Met	Absent	Absent	Absent	Absent	Absent	Absent	Absent	Absent	Absent	Absent
13	26/F	Val30Met	Normal	Absent	35 m/s	7.0 ms	1.5 mV	Absent	Absent	Absent	Absent	Absent
14	58/M	Ile107Val	Delayed	Absent	43 m/s	5.2 ms	0.3 mV	29.4 m/s	8.2 ms	0.3 mV	Absent	Absent
15	59/M	Val30Met	Absent	Absent	42 m/s	4.79 ms	3.4 mV	42 m/s	5.43 ms	6.0 mV	Absent	Absent
16	62/M	Val30Met	Delayed	Delayed	Absent	Absent	Absent	41 m/s	4.8 ms	2.2 mV	Absent	Absent
17	59/M	Val30Met	Normal	Delayed	27.4 m/s	7.5 ms	0.4 mV	34 m/s	5.9 ms	0.77 mV	Absent	Absent
18	58/M	Leu78His	Normal	Absent	Absent	Absent	Absent	Absent	Absent	Absent	Absent	Absent
19	64/M	Thr60Ala	Absent	Absent	Absent	Absent	Absent	Absent	Absent	Absent	Absent	Absent
20	48/M	Glu54Gln	N/A	Absent	35 m/s	6.26 ms	2.9 mV	40 m/s	5.03 ms	6.6 mV	Absent	Absent

CMAP = compound muscle action potential; DML = distal motor latency; NCV = nerve conduction studies; SNAP = sensory nerve action potential; SSR = sympathetic skin response.

Magnetic resonance neurography protocol

All participants were examined supine and with feet first in a 3.0 T MR Scanner (Magnetom TIM TRIO, Siemens Healthcare). The following extensive imaging protocol was carried out. It provided large anatomical coverage for each leg and at the same time high structural resolution:

(i) 3D T_2-weighted inversion-recovery SPACE (Sampling Perfection with Application optimized Contrasts using different flip angle Evolution) sequences for imaging of the lumbar plexus and spinal nerves with axial reformations (50 axial images/patient): repetition time/echo time 3000/202 ms, field of view $305 \times 305\,mm^2$, matrix size $320 \times 320 \times 104$, slice thickness 1.0 mm, no gap, voxel size $1.0 \times 1.0 \times 1.0\,mm^3$, acquisition time 8:32 min.

(ii) Axial high-resolution T_2-weighted turbo spin echo 2D-sequences with spectral fat-saturation (three slabs per leg, equalling six slabs per subject). Slab 1: proximal thigh to mid-thigh; Slab 2: lower leg with alignment of the proximal edge of this imaging slab on the tibiofemoral joint space; Slab 3: ankle-level with alignment of the distal edge of this imaging-slab on the tibiotalar joint space. Repetition time/echo time 5970/55 ms, field of view $150 \times 150\,mm^2$, matrix size 512×512, slice thickness 3.5 mm, interslice gap 0.35 mm, voxel size $0.4 \times 0.3 \times 3.5\,mm^3$, 35 slices, acquisition time per slab 4:42 min.

(iii) Axial high-resolution dual echo turbo spin echo 2D sequence with spectral fat saturation (one slab per leg, equalling two slabs per subject): mid-thigh to distal thigh with alignment of the distal edge of this imaging-slab on the tibiofemoral joint space. Repetition time 5210 ms, echo $time_1$/echo $time_2$ 12/73 ms, field of view $150 \times 150\,mm^2$, matrix size 512×512, slice thickness 3.5 mm, interslice gap 0.35 mm, voxel size $0.4 \times 0.3 \times 3.5\,mm^3$, 35 slices, acquisition time per slab 7:30 min. The net imaging time including survey scans was 52:13 min. Patient and coil repositioning required additional time, resulting in a total examination time of 80–90 min per subject. A 4-channel body-array flex-coil (Siemens Healthcare) was used for imaging of the lumbar plexus (Sequence 1), and a 15-channel Transmit-Receive extremity-coil (INVIVO) for imaging of the complete right and left leg, respectively.

Image and statistical analyses

Image processing and segmentation

Image data pseudonymization and standard file format conversation were performed for further image processing and analysis [DICOM (Digital Imaging and Communications in Medicine) to NIFTI (Neuroimaging Informatics Technology Initiative) using the software MRIConvert]. Image processing and analysis was performed in FSL, a comprehensive software library for the statistical analysis of neuroimaging data (Jenkinson *et al.*, 2012). All images from proximal thigh to distal ankle were merged into one image stack for each leg (140 axial image slices per leg, 280 per subject). On each axial imaging slice, the tibial and peroneal fascicles of the sciatic nerve and their distal continuation as either tibial or common peroneal nerve down to ankle level were identified and manually segmented by one neuroradiologist with 5 years of experience in MR-neurography (J.K.). The contour between nerve fascicles and epineurium, served as reliably visible segmentation border. Two different nerve-voxel territories were stored separately after manual segmentation as regions of interest: (i) tibial fascicles and their distal continuation as tibial nerve; and (ii) peroneal fascicles and their distal continuation as common peroneal nerve. Slice numbering was from 0 (most proximal slice located at proximal thigh level) to 139 (most distal slice located at level of the tibiotalar joint space) for the tibial nerve. For the common peroneal nerve slice numbering was from 0 (proximal thigh) to 60 (level of the fibular head). Peroneal branches distal to the common peroneal nerve were not reliably recognizable in all subjects and therefore were not analysed.

Normalization of signal intensity and statistical lesion classification

All voxels within tibial and peroneal regions of interest were considered 'nerve voxels' or 'nerve–tissue voxels'. Lesion classification, i.e. the binary classification of 'nerve voxels' as 'nerve–lesion voxels' was performed by comparing the normalized frequency distributions of signal intensities for all 'nerve-voxels' within a certain region of interest between the healthy age- and sex-matched controls and patients or gene carriers. Specifically, for each slice position, for each nerve region of interest (tibial or peroneal) and for each side (right or left), the robust signal intensity range (2–98 percentile range) was divided into 100 bins of equal width. Then, the number of voxels occurring within each bin-class was computed for each subject and for each and every slice position, nerve (tibial or peroneal) and side (right or left). The bin class containing the highest number of 'nerve-voxels' (i.e. the histogram peak) in the age- and sex-matched control group (per position/nerve/slice) served as reference bin for intensity normalization. For the purpose of intensity normalization, each bin class (for each subject/position/nerve/side/slice) was divided by the bin class at which the histogram peak occurred in the age- and sex-matched control group (within the same respective slice/nerve/side). As a result, the histograms (nerve voxel frequency distribution of signal intensities within 100 bins) of all subjects were centred around the histogram peak of the age- and sex-matched control population. We intentionally made no assumptions on a certain threshold of normalized bin classes to serve as cut-off value for binary classification ('nerve–lesion voxels' versus 'non-lesion–nerve voxels') but chose the threshold that best provided a separation between the three groups. At a cut-off value of >1.2 (normalized signal intensity), the group differences (controls versus asymptomatic carriers versus symptomatic patients) in 'nerve–lesion voxels' were maximized. In other words, all 'nerve voxels' falling, according to their signal intensities into normalized bin classes, >1.2 were classified as 'nerve-lesion-voxels'. The absolute count of these 'nerve–lesion voxels' was automatically computed and denominated as 'nerve–lesion voxel number' (per slice position) or total 'nerve–lesion voxel count' (cumulative lesion voxel number over all slices from proximal to distal).

Lesion load: proximal to distal cumulation of lesion voxel count

The total nerve–lesion voxel number was determined by cumulating all lesion voxels from proximal to distal (Fig. 1). This total lesion voxel number was statistically compared between

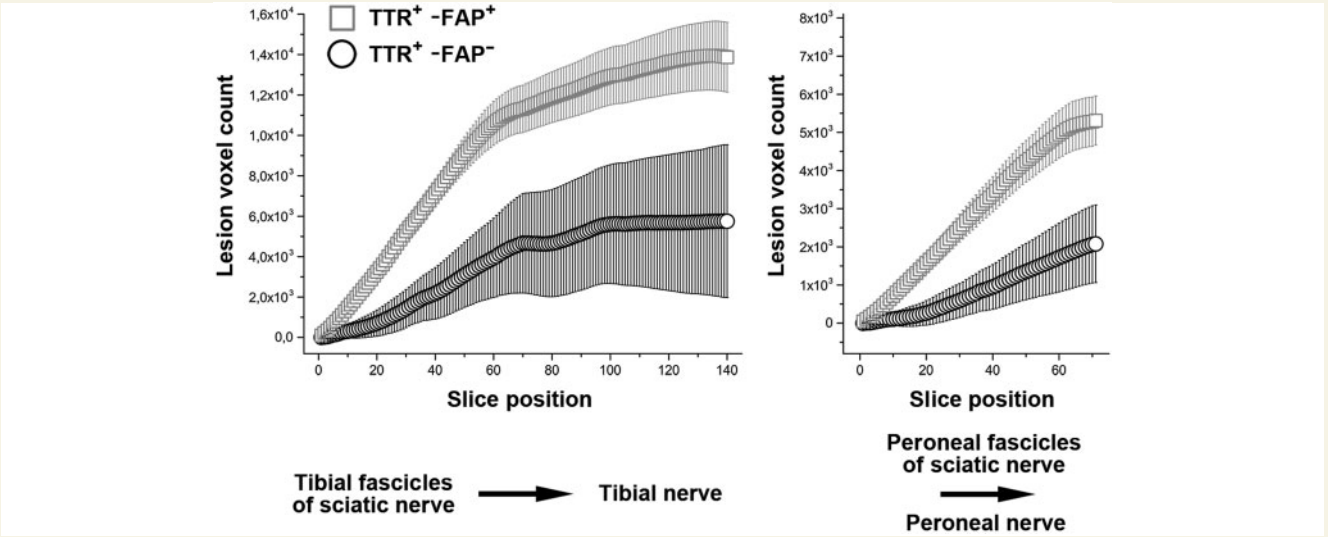

Figure 1 Cumulated nerve lesion count. Cumulated nerve–lesion voxel number from proximal-to-distal for the tibial fascicles within the sciatic nerve and their distal continuation as tibial nerve (*left*, slice positions 0 to 139), and for the peroneal fascicles within the sciatic nerve and their distal continuation as common peroneal nerve (*right*, slice positions 0 to 69). Mean frequencies of nerve–lesion voxels numbers were calculated and referenced to the control group which was set as baseline. Note the marked increase in the cumulated lesion voxel numbers in manifest TTR-FAP (TTR^+-FAP^+, squares). Lesion voxel number in asymptomatic gene carriers (TTR^+-FAP^-, circles) revealed also strong statistical differences compared to symptomatic TTR-FAP patients, as well as compared to the healthy volunteers.

the three groups (symptomatic TTR-FAP versus asymptomatic gene carriers versus healthy controls) by using the Wilcoxon's rank sum test. Preliminary analyses had shown that within each group, no statistical differences existed between lesion voxel numbers of right and left legs. Therefore, for each slice position (0–139) and for each nerve territory (tibial and peroneal) lesion voxel numbers of right and left sides were averaged.

Proximal to distal mapping of anatomical lesion localization

Besides evaluation of the total nerve–lesion voxel number, which is devoid of spatial and localization information, a proximal to distal anatomical mapping of lesion voxels was performed by plotting mean lesion voxel numbers per slice position and within each group (Fig. 2). A two-way repeated measures ANOVA was then performed to analyse the effects of Group (symptomatic TTR-FAP versus asymptomatic gene carriers versus controls) and anatomical Location (proximal versus distal). Proximal and distal as the two factor levels of Location were represented by the mean lesion voxel number averaged over slices 0–69 (proximal) and slices 70–139 (distal).

Signal quantification: T_2 relaxation time and spin density at thigh level

The additionally performed signal quantification required the recording of the MR signal at varying echo times. To keep the total acquisition time reasonable, signal quantification was only achieved at one image slab level per leg (distal thigh) by using a dual turbo spin echo sequence. We elected the thigh level for signal quantification because preliminary data in few TTR-FAP patients revealed strongest nerve–lesion conspicuity just at this anatomical region. The two quantitative

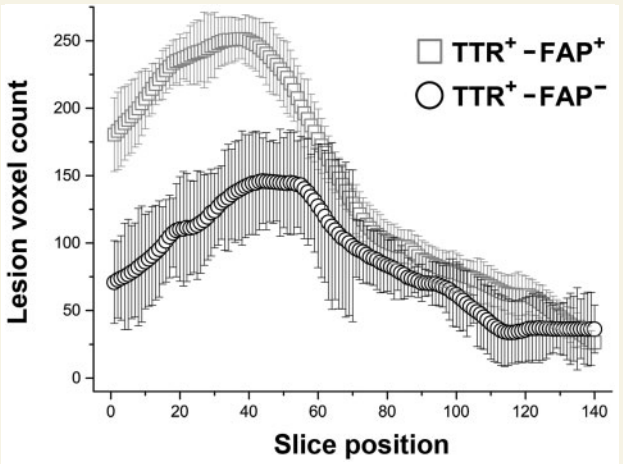

Figure 2 Lesion localization. Proximal to distal mapping of lesion-voxels-numbers within the tibial nerve [slice positions 0 (= proximal thigh) to 139 (= tibiotalar joint)]. Mean frequencies of lesion voxel number within the tibial nerve were calculated and referenced to the control group which was set as baseline. Note the predominant and statistically significant proximal focus of nerve lesions at thigh level in both, the manifest TTR-FAP patients (TTR^+-FAP^+, squares) and the asymptomatic gene carriers (TTR^+-FAP^-, circles). Differences in the proximal lesion voxel number between manifest TTR-FAP and gene carriers were also highly significant.

estimates, apparent T_2 relaxation time [T_{2app}, Equation (1)] and proton spin density [ρ, Equation (2)], both known to be distinct and quantifiable parameters that measure the microstructural nerve-tissue composition *in vivo*, were calculated for all nerve–lesion voxels according to the following formulas

(Heiland *et al.*, 2002):

$$T_{2app} = \frac{TE_2 - TE_1}{\ln(SI(TE_1)/(SI(TE_2))} \quad \text{(Equation 1)}$$

$$\rho = \frac{SI(TE_1)}{\exp(-TE_1/T_{2app})} \quad \text{(Equation 2)}$$

Quantification of nerve calibre

Nerve calibre was quantified by calculating cross-sectional areas for tibial and peroneal nerve regions of interest. Tibial regions of interest were analysed over all 140 slices. A two-way repeated measures ANOVA was performed to analyse the effects of Group (symptomatic TTR-FAP versus asymptomatic gene carriers versus controls) and anatomical Location (proximal versus distal) on the calibre of tibial fascicles (no such analysis was performed for peroneal regions of interest as only tibial regions of interest could be tracked until the far distal ankle level). Proximal and distal as the two factor levels of Location were represented by the mean tibial nerve calibre averaged over proximal slices (0–69) and distal slices (70–139). A one-way ANOVA was performed to analyse the effect of Group on the calibre of peroneal fascicles.

Lesion analysis at far proximal level: lumbosacral plexus and spinal nerves

On axial reformations of sequence 1, bilateral spinal nerves L5 and S1 and their corresponding dorsal root ganglia, as well as the lumbosacral plexus at level of the sciatic notch on either side, were manually segmented. Signal normalization was performed by calculating signal ratios between nerve regions of interest and adjacent muscle (ipsilateral psoas muscle for L5 and S1 and ipsilateral piriformis muscle for plexus region of interest). Preliminary analyses showed that within each group (symptomatic TTR-FAP, asymptomatic gene carriers, healthy controls), no statistical differences existed between the right and left side of spinal nerve and plexus regions of interest. Averaged signal ratios were eventually analysed by one-way ANOVA for an effect of Group. All *P*-values for *post hoc* contrasts were corrected for multiple comparisons by the method of Scheffé (Enderlein, 1961).

Results

Clinical and genetic data

Asymptomatic carriers of any mutation in the *TTR* gene

Four of seven asymptomatic gene carriers were found to have the Val30Met mutation of the *TTR* gene, the most common mutation underlying an early manifestation of polyneuropathy (Table 1). The remaining three gene carriers either exhibited the Leu58His or Tyr69His mutation.

Absence of symptomatic polyneuropathy in these seven subjects was confirmed by detailed clinical neurological examinations and a score of 0 in Neuropathy Symptom Score, Neuropathy Deficit Score and Neuropathy Impairment Score–lower limbs (Table 1). One patient in this group was suffering from mild aphasia due to focal meningeal amyloidosis confirmed by brain MRI (Table 1). Other organ manifestations of TTR-FAP were excluded in all asymptomatic carriers. Electrophysiological examinations were completely normal in all seven asymptomatic carriers of the *TTR* gene, except for slightly reduced sural sensory nerve action potential in three cases (Table 2).

Symptomatic TTR-FAP

The Val30Met mutation was underlying in 7 of 13 symptomatic patients. A summary of other causative point mutations in the remaining six patients, as well as age and symptoms at onset, familiarity, associated symptoms and Neuropathy Symptom Score, Neuropathy Deficit Score, Neuropathy Impairment Score–lower limbs grading for all 13 patients are given in Table 1. In this group patients suffered mainly from sensory symptoms in the lower limbs such as numbness, painful paraesthesia, loss of temperature sensation and—in severe cases—loss of motor strength. Patients also presented with additional non-polyneuropathic symptoms, such as cardiac, gastrointestinal and autonomic manifestations, and with carpal tunnel syndrome (Table 1). Nerve conduction studies revealed pathological peroneal nerve compound muscle action potentials in 13 of 13 cases and pathological tibial nerve compound muscle action potentials in 11 of 13 cases. Furthermore, in 6 of 13 cases (peroneal nerve) and 5 of 13 cases (tibial nerve) a complete loss of electrical nerve conduction with absence of compound muscle action potentials and in 13 of 13 cases (sural nerve) absence of sensory nerve action potentials were detected, both related to a substantial loss of all fibre classes. Detailed results of motor and sensory nerve conduction studies and sympathetic skin response are presented in Table 2.

Magnetic resonance neurography: lesion detection by statistical voxel classification

Lesion load: sciatic nerve (tibial fascicles) and tibial nerve continuation

For tibial fascicles of the sciatic nerve and their distal continuation as tibial nerve down to ankle level, the total nerve–lesion voxel number was significantly higher in symptomatic TTR-FAP ($20\,405 \pm 1586$), than in healthy controls (6536 ± 467; $P < 0.0001$; Figs 1 and 4). In asymptomatic gene carriers ($12\,294 \pm 3199$) the total tibial nerve–lesion voxel number was also significantly higher than in healthy controls ($P = 0.043$), but significantly lower than in symptomatic TTR-FAP ($P = 0.036$).

Lesion load: sciatic nerve (peroneal fascicles) and common peroneal nerve continuation

For peroneal fascicles within the sciatic nerve and their distal continuation as common peroneal nerve down to the level of the fibular head, the total nerve–lesion voxel number was significantly higher in symptomatic TTR-FAP

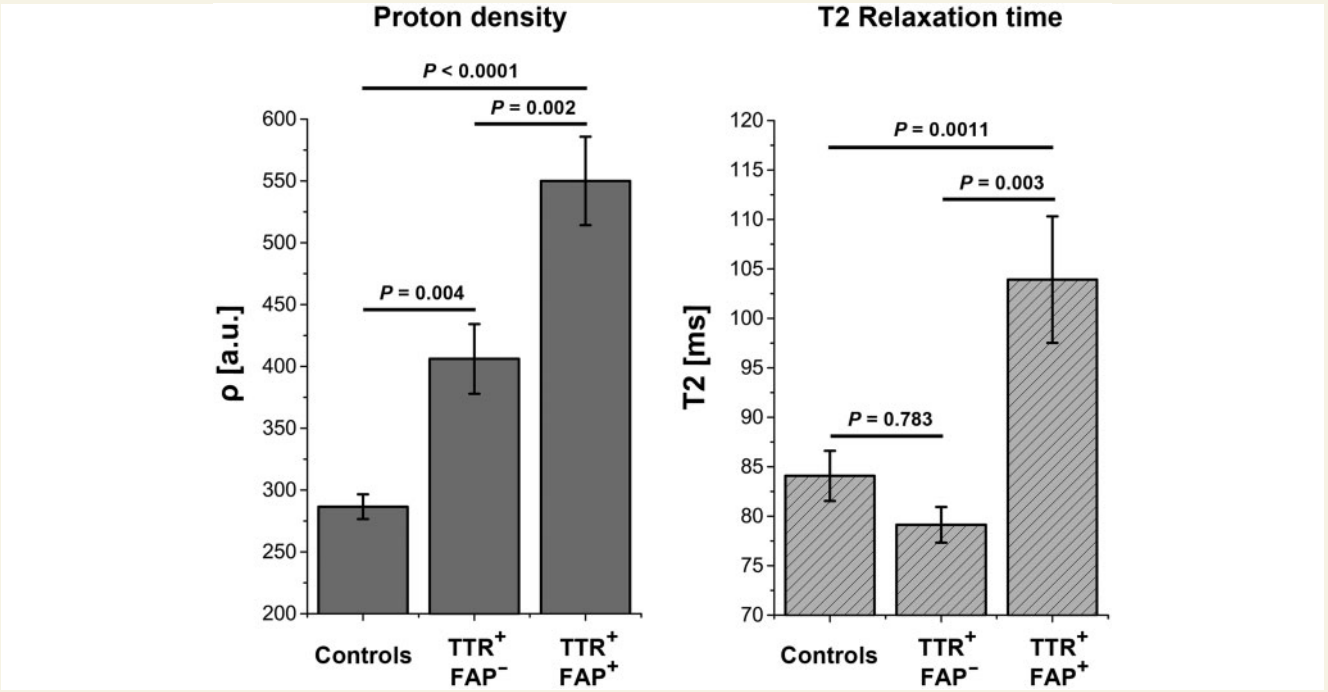

Figure 3 Signal quantification. Quantification of mean proton spin density (ρ) and T_2 relaxation time (T_{2app}) at thigh level, the site of predominant lesion focus plotted for each group. Differences in ρ (*left*) were highly significant between all three groups: manifest TTR-FAP versus asymptomatic gene carriers ($P = 0.002$); manifest TTR-FAP versus controls ($P < 0.0001$); asymptomatic gene carriers versus controls ($P = 0.004$). Significant differences were also found in T_{2app} between manifest TTR-FAP and asymptomatic gene carriers ($P = 0.003$) and between manifest TTR-FAP and controls ($P = 0.0011$) but not between asymptomatic gene carriers and controls ($P = 0.783$), indicating that ρ has higher sensitivity in detecting early nerve injury, whereas T_{2app} may better differentiate between increasing severity of clinical nerve impairment. TTR^+-FAP^+ = manifest/symptomatic TTR-FAP; TTR^+-FAP^- = asymptomatic gene carriers.

(9171 ± 750), than in healthy controls (2759 ± 170; $P < 0.0001$; Figs 1 and 4). In asymptomatic gene carriers (5622 ± 837) the total peroneal nerve–lesion voxel number was also significantly higher than in healthy controls ($P = 0.0017$), but significantly lower than in symptomatic TTR-FAP ($P = 0.0202$).

Lesion localization: distribution of nerve–lesion voxels from proximal to distal

Only the tibial fascicles within the sciatic nerve and their continuation as the tibial nerve can be tracked from proximal down to ankle level. For this anatomical reason, the following ANOVA was only carried out for tibial fascicles and their distal continuation as tibial nerve and not for peroneal fascicles or common peroneal nerve, respectively.

Two-way ANOVA with between-subjects factor Group (symptomatic TTR-FAP versus asymptomatic gene carriers versus controls) and within-subjects factor Location (proximal versus distal) was significant each for Group (f-value = 60.33, $P < 0.0001$) and Location (f-value = 279.22, $P < 0.0001$). *Post hoc* pairwise contrasts indicated that the average nerve–lesion voxel number per slice was significantly higher for symptomatic TTR-FAP than for asymptomatic carriers ($P = 0.003$, corrected by the Scheffé method), was significantly higher for asymptomatic carriers than for controls ($P = 0.035$, corrected), and was significantly higher for symptomatic TTR-FAP than for controls ($P < 0.0001$, corrected). *Post hoc* pairwise contrasts also showed that the mean proximal nerve–lesion voxel number over all groups was largely and significantly higher than the mean distal nerve–lesion voxel number ($P < 0.0001$, corrected).

The effect of interaction between Location and Group was also strongly significant: f-value=99.7, $P < 0.0001$. *Post hoc* pairwise comparisons indicated a steeper proximal to distal lesion gradient with the manifestation of symptomatic disease: the mean proximal nerve–lesion voxel number per slice was more severe in symptomatic TTR-FAP than in asymptomatic carriers of the *TTR* gene ($P = 0.001$, corrected).

The mean number of nerve–lesion voxels per slice position is mapped for each group in Fig. 2 from the most proximal slice (position 0 at proximal thigh) to the most distal slice (position 139 at ankle level).

Magnetic resonance neurography: signal quantification at the site of predominant injury

One-way ANOVA revealed significant differences between groups for the quantified spin-density ρ (f-value = 50.95,

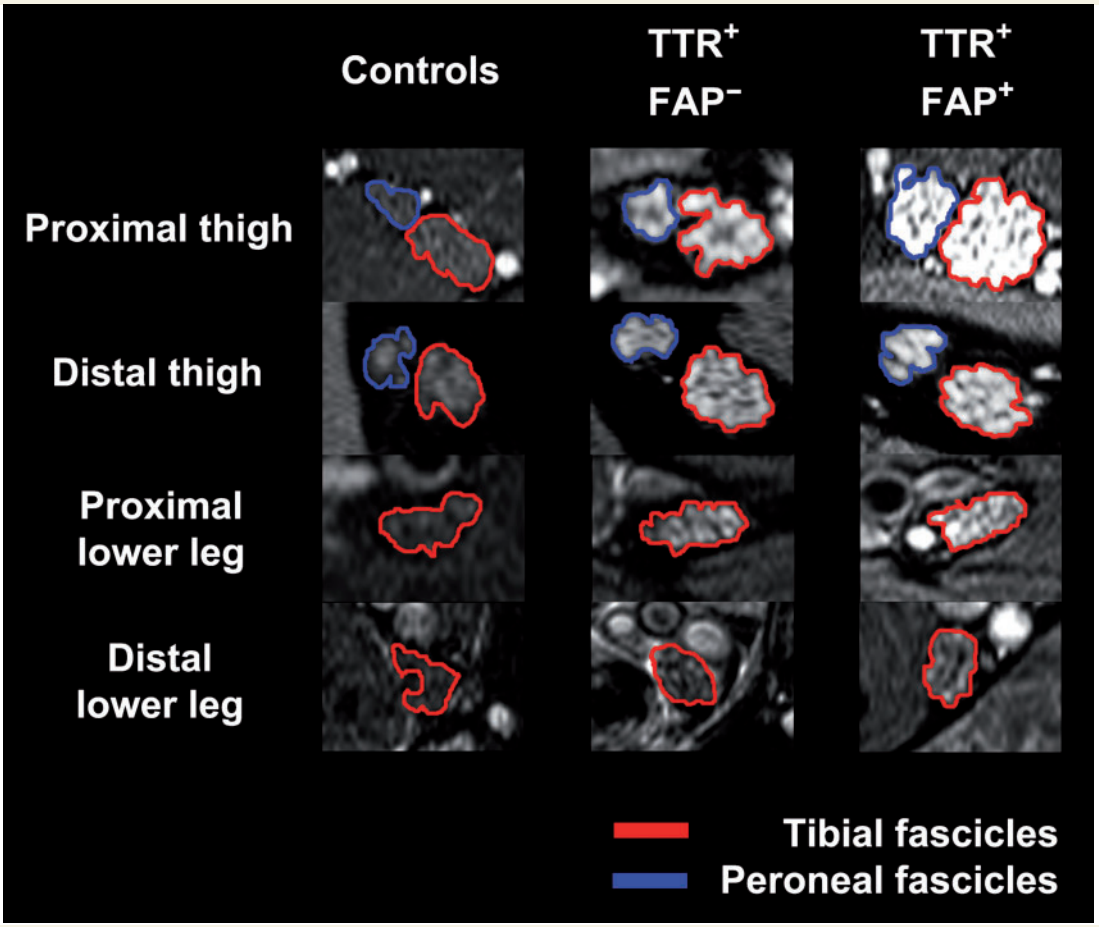

Figure 4 Magnetic resonance neurography source images. Representative source images (right leg; high-resolution T_2-weighted turbo spin echo fat-saturated sequences, 3 T) with overlaid coloured regions of interest indicating segmented tibial and peroneal fascicles within the sciatic nerve (at proximal thigh and distal thigh levels) and the distal continuation of tibial fascicles as tibial nerve (at proximal lower leg and distal lower leg levels). One healthy control, an asymptomatic gene carrier (TTR^+-FAP^-) and a manifest TTR-FAP patient (TTR^+-FAP^+) at equal slice positions are shown. Nerve lesions and nerve calibre increase are apparent already in the asymptomatic group but not in controls. Further increase in lesion contrast and calibre is observed in manifest TTR-FAP. Nerve-lesion contrast and nerve calibre show a clear proximal focus at thigh level in both TTR-FAP groups, indicating that nerve injury in distally-symmetric TTR-FAP starts and progresses at this proximal site of the peripheral nervous system. Tibial fascicles within the sciatic nerve and tibial nerve, respectively (encircled in red); peroneal fascicles within the sciatic nerve (encircled in blue).

$P < 0.0001$). *Post hoc* comparisons showed that ρ was highest in symptomatic TTR-FAP (549.97 ± 35.78), decreased significantly in asymptomatic gene carriers (406.09 ± 28.22; $P = 0.002$), and further decreased significantly in healthy controls (286.56 ± 10.04; $P < 0.0001$ versus symptomatic TTR-FAP and $P = 0.004$ versus asymptomatic gene carriers, all *P*-values after Scheffé correction).

One-way ANOVA also revealed significant differences between groups for the apparent T_2-relaxation-time T_{2app} (f-value = 7.64; $P = 0.0011$). *Post hoc* comparisons showed that T_{2app} was significantly increased only in symptomatic disease (symptomatic TTR-FAP 103.92 ± 6.4 ms versus asymptomatic gene carriers 79.14 ± 1.8 ms, $P = 0.012$ and versus healthy controls 84.08 ± 2.54 ms, $P = 0.003$; both *P*-values Scheffé corrected). However, no significant difference of T_{2app} was observed between asymptomatic gene carriers and controls ($P = 0.783$). Mean ρ and T_{2app} are plotted for each group in Fig. 3.

Quantification of nerve calibre

The mean cross-sectional area of tibial fascicles within the sciatic nerve and their distal continuation as tibial nerve was significantly different between Group (f-value = 23.50, $P < 0.0001$) and Location (f-value = 425.69, $P < 0.0001$). *Post hoc* contrasts showed that (i) cross-sectional area was larger proximally irrespective of group ($P < 0.0001$, corrected), and that irrespective of their location; (ii) cross-sectional area was significantly larger in symptomatic TTR-FAP (75.47 ± 10.45 mm^2) versus

controls (53.63 ±2.19 mm^2, $P < 0.0001$); and (iii) cross-sectional area was also larger between symptomatic TTR-FAP and asymptomatic gene carriers (65.70 ± 9.54 mm^2), however differences between these two groups were not statistically significant ($P = 0.182$).

Importantly, as in the lesion-voxel analyses, the interaction between Group and Location was also significant for nerve calibre (f-value 67.88; $P < 0.0001$). This effect of interaction indicates that independent from the natural anatomical effect of proximally increasing calibre (main effect of Location) and independent from the apparent disease related calibre increase (effect of Group), there exists an additional location dependent effect of disease severity on nerve calibre. *Post hoc* contrasts indicated that the magnitude of proximal but not of distal calibre gain increased significantly over groups: (i) symptomatic TTR-FAP versus asymptomatic gene carriers (108.54 ± 5.80 mm^2 versus 85.16 ± 7.46 mm^2, $P = 0.006$); (ii) symptomatic TTR-FAP versus controls (108.54 ± 5.83 mm^2 versus 64.02 ± 1.80 mm^2, $P < 0.0001$); and (iii) asymptomatic gene carriers versus controls (85.16 ± 7.46 mm^2 versus 64.02 ± 1.80 mm^2, $P = 0.004$).

The mean cross-sectional area of peroneal fascicles within the sciatic nerve and their distal continuation as common peroneal nerve showed similar differences. Because analysis of the common peroneal nerve did not proceed further distally than knee level, only one-way ANOVA was performed to test for an effect of Group: f-value = 26.11, $P < 0.0001$. *Post hoc* contrasts showed that peroneal fascicles were largest in symptomatic TTR-FAP (40.50 ± 1.84 mm^2), significantly smaller in asymptomatic gene carriers (34.41 ± 3.09 mm^2, $P = 0.023$), and also significantly smaller in controls (27.96 ± 0.74 mm^2, $P < 0.0001$). The difference between asymptomatic gene carriers and controls was not statistically significant ($P = 0.074$).

Analyses at far proximal level: spinal nerves and lumbosacral plexus

Signal ratios were significantly different between groups (f-value 12.05, $P < 0.0001$). *Post hoc* contrasts revealed significantly higher signal ratios in symptomatic TTR-FAP (3.29 ± 0.27) versus controls (2.37 ± 0.09, $P < 0.0001$ corrected); and in asymptomatic gene carriers (3.26 ± 0.17) versus controls (2.37 ± 0.09, $P = 0.008$ corrected). No difference was observed between symptomatic TTR-FAP and asymptomatic carriers ($P = 0.996$, corrected).

Nerve calibre was significantly different between groups (f-value = 146.33, $P < 0.0001$). *Post hoc* contrasts revealed significantly larger calibre in symptomatic TTR-FAP (37.0 ± 1.9 mm^2) versus controls (14.9 ± 0.5 mm^2, $P < 0.0001$ corrected); in asymptomatic gene carriers (29.6 ± 1.6 mm^2) versus controls (14.9 ± 0.5 mm^2, $P < 0.0001$ corrected); and also in symptomatic TTR-FAP versus asymptomatic gene carriers ($P = 0.002$, corrected).

Histopathology: sural nerve biopsies

Sural nerve biopsy was available in 8 of 13 patients with symptomatic TTR-FAP. In four nerve specimens of severely affected patients, variable amounts of TTR-amyloid were detectable in the endo- and perineurial compartment (Fig. 5). The remaining four biopsies were obtained from manifest TTR-FAP patients with moderate polyneuropathy and showed no amyloid deposits.

Discussion

TTR-FAP is a rare polyneuropathy with autosomal-dominant inheritance and exhibits a clinical phenotype with distally-symmetric symptoms. The quality of symptoms indicates small fibre injury especially early during disease manifestation. In contrast to other polyneuropathies, the initial pathomechanism, which is a point mutation in the *TTR* gene, is well understood. As a consequence, an increasing armamentarium of effective therapeutic strategies is emerging (Tojo *et al.*, 2006; Coelho *et al.*, 2012, 2013; Hund, 2012; Johnson *et al.*, 2012; Berk *et al.*, 2013). However, the early and objective recognition and localization of nerve injury remain difficult.

We report that lower limb peripheral nerve injury in TTR-FAP is detectable, can be localized and quantified with high spatial accuracy *in vivo* by high resolution MR-neurography. Using this imaging method, nerve injury was reliably detected with strong lesion contrast even before the manifestation of symptomatic disease in asymptomatic carriers with confirmed disease-causing mutations of the *TTR* gene (Val30Met, Leu58His or Tyr69His). At the heart of our study, we used this method with an extensive imaging protocol providing high-spatial resolution to facilitate the precise manual segmentation of nerve–tissue voxels, and very large proximal to distal anatomical coverage of both lower extremities (2 × 140 slices) including spinal nerves and lumbosacral plexus (additional 50 slices). In the same manner, we also collected data in a large age- and sex-matched normative healthy cohort for the purpose of statistical classification of nerve–lesion voxels in the asymptomatic and symptomatic groups of TTR-FAP, which were both graded by established clinical and electrophysiological scores. Coverage over large regions of the lower extremity peripheral nervous system allowed us to identify the localization and dispersion of nerve lesions along the entire leg. Nerve lesions as observed by imaging occurred in a non-diffuse pattern with a clear focus at the thigh level where nerve injury was strongest. At this location, proton spin density (ρ) and T_{2app} were calculated as two distinct and quantifiable *in vivo* tissue parameters of microstructural integrity. These parameters help to further specify the microstructural sources that contribute to the pathological MR signal increase, measured as nerve–lesion voxel number. At thigh level, alterations of these quantitative markers were found

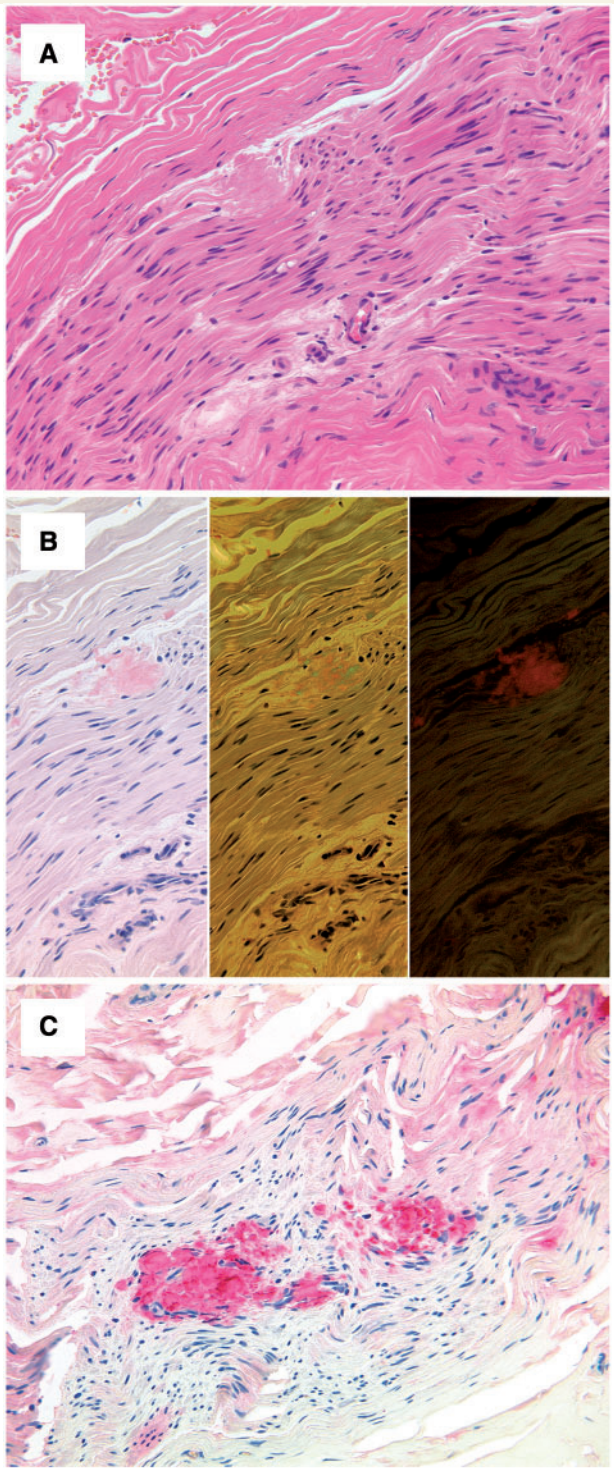

Figure 5 Histopathology. Sural nerve biopsy of a male patient showing peri- and endoneural amyloid deposits with a homogeneous eosinophilic appearance in haematoxylin and eosin-stained sections (**A**). Congo red staining yields a pale red staining in bright light (**B**, *left*), apple green birefringence in polarized light (**B**, *middle*) and an orange fluorescence in fluorescence microscopy (**B**, *right*). Immunostaining with an antibody directed against transthyretin shows a strong and even immunoreaction of the amyloid deposits (**C**).

to be highly specific for each group: (i) asymptomatic carrier status and symptomatic disease were both closely associated with a strong increase of proton spin density (ρ); and (ii) a significant increase of the T_2 relaxation time (T_{2app}) was found only in symptomatic TTR-FAP, but not in asymptomatic carriers. These findings suggest that ρ is more sensitive for the detection of early or even subclinical lesions, whereas T_{2app} may serve to specifically differentiate increasing disease severity in already symptomatic TTR-FAP.

This study in TTR-FAP, which is a rare disease occurring in 0.1:100 000 persons per year (Benson, 1995), was cross-sectional and not longitudinal. Therefore, any interpretation about the temporal evolution of the observed MR markers must remain limited. Nevertheless, the quantitative MR estimates are likely to be linked to the manifestation of symptoms and clinical disease progression over time, because their alterations were highly specific for asymptomatic gene carriers (only increase in ρ) and symptomatic TTR-FAP (increase in both ρ and T_{2app}). Furthermore, the observed lesion pattern was clearly non-diffuse in that the thigh level could be identified as the site of predominant injury. This effect of location-dependent injury interacted with the stage of disease (Group factor), suggesting that progressive proximal structural injury at thigh level is linked to clinical manifestation and severity.

The diagnostic value of measuring even early nerve injury may include earlier initiation of established causative therapies, but also earlier recognition of beneficial effects in clinical intervention studies. Previously, early liver transplantation was the only causative therapy in TTR-FAP (Holmgren *et al.*, 1991; Reilly, 2005). Long-term outcomes showed that further disease progression is halted after liver transplantation, but reversal of symptoms or improvement of electrophysiological findings typically has not been observed over time after this substantially invasive intervention (Holmgren *et al.*, 1993; Bergethon *et al.*, 1996; Adams *et al.*, 2000). Only recently, promising results for the transthyretin stabilizing drugs tafamidis meglumine and diflunisal have been published, also showing the beneficial effect that clinical disease progression is slowed or even halted when administration started on time (Coelho *et al.*, 2012; Berk *et al.*, 2013). However, as in the case of liver transplantation, early diagnosis followed by timely intervention was shown to be of utmost importance, because both drugs were not able to substantially reverse functional deficits (Coelho *et al.*, 2012; Berk *et al.*, 2013; Merlini *et al.*, 2013). Furthermore, to date, tafamidis is licensed only in patients who do not require any walking assistance (stage I TTR-FAP) (Coutinho *et al.*, 1980; Reilly, 2005). Several other new treatment options are emerging with promising results, e.g. doxycycline, or RNAi therapy (Tojo *et al.*, 2006; Hund, 2012; Ando *et al.*, 2013; Coelho *et al.*, 2013). An early, objective monitoring of beneficial therapeutic effects on functional and structural nerve impairment is needed to better evaluate the effectiveness of any novel therapeutic agent in halting progression or

reversing nerve injury in TTR-FAP. Nerve conduction studies represent the diagnostic gold standard for the assessment of electrical function of large myelinated fibres in peripheral nerves; however, nerve conduction studies are limited as long as small fibre injury predominates, which presumably occurs during early stages of TTR-FAP (Thomas and King, 1974; Said *et al.*, 1984; Plante-Bordeneuve and Said, 2011).

In patients with severely symptomatic disease, nerve conduction studies come with another important limitation. The profound loss of all fibre classes including large myelinated fibres typically leads to a complete loss of electrical nerve conduction with non-measurable compound muscle action potential and sensory nerve action potential. In these patients an objective and reliable determination of any further clinical deterioration may be problematic. Therefore, it is difficult in advanced disease to assess the effect of any particular therapeutic intervention. Early recognition of nerve injury, when small fibre loss prevails and staging of advanced disease associated with severe loss of all fibre classes seem promising by monitoring specific alterations of the two quantitative imaging markers observed in this study. It is important to emphasize that direct imaging of small fibres is not possible by MR-neurography, at least to date, and was not accomplished here. However, high structural resolution allowed us to recognize that lesion contrast emerges from the nerve fascicles (Fig. 4). So we may assume that the observed lesions reflect the sum of injury in the fascicular compartment including both small fibres and large myelinated fibres and importantly, also the extracellular space of the endoneurial compartment.

It remains difficult to interpret which structural changes of the nerve fascicles lead to alterations in ρ and T_{2app} *in vivo*. A direct correlation between peripheral nerve imaging and histopathology is difficult to achieve in general. In particular, at proximal sites where strongest injury was observed, fascicle biopsies of the sciatic nerve are not possible and therefore are restricted to the distal sural nerve. Facing these methodological restrictions, any further interpretation about the microstructural sources underlying ρ and/or T_{2app} increase therefore remains limited to theoretical considerations. The increase of ρ observed in symptomatic TTR-FAP patients and asymptomatic gene carriers, points toward a change in the macromolecular organization of the extracellular compartment (Davies *et al.*, 2003) as it occurs by extracellular deposition of mutant transthyretin within the endoneurial compartment. The additional increase of T_{2app}, which was observed specifically only in symptomatic TTR-FAP, indicates an increase of free-water protons as it would occur in endoneurial oedema (Tofts and du Boulay, 1990; Abbas *et al.*, 2014).

TTR-FAP manifests with distally symmetric symptoms similar to the clinical appearance of other polyneuropathies, such as diabetic polyneuropathy (Kelly *et al.*, 1979; Hund *et al.*, 2001; Reilly, 2005). However, nerve lesions as detected by MR-neurography appeared with a strong proximal focus centred at thigh level and were in strong contrast to lesser injury at more distal levels (lower leg and ankle). This finding was further supported by a clear pathological proximal nerve calibre increase as another target measure which is merely morphometric and therefore relatively independent from MR signal alterations.

Altogether, it remains unclear how proximal nerve injury at proximal level of the lower extremity peripheral nervous system translates into distally symmetric symptoms and into distal fibre loss as the prominent and undisputed pathohistological fingerprint of advanced disease (Van Allen *et al.*, 1969; Thomas and King, 1974; Rajani *et al.*, 2000; Plante-Bordeneuve and Said, 2011). One possible explanation may be that distal fibre loss is preceded by the accumulation of nerve injury at more proximal levels possibly triggering, in a length-dependent manner, the loss of distal fibres. This explanation was offered previously by Dyck and colleagues (Sugimura and Dyck, 1982; Dyck *et al.*, 1986*a*, *b*; Dyck and Norell, 1999) on the basis of their meticulous histological work in diabetic polyneuropathy. These authors observed in invaluable human specimens post-mortem or after limb amputation, that proximal injury is focused at thigh level and may accumulate in a multifocal pattern and thereby possibly trigger distal fibre loss. These *ex vivo* findings have been supported recently by a preliminary imaging study showing similar proximal nerve lesions in sciatic nerves at thigh level in patients with prototypical distally-symmetric diabetic polyneuropathy (Pham *et al.*, 2011). Histopathological studies in amyloid polyneuropathies report a severe fibre loss, degeneration of myelinated fibres and amyloid deposits in the sciatic nerve and the dorsal root ganglia and therewith also in proximal regions of the lower extremity peripheral nervous system (De Navasquez, 1938; Andrade, 1952; Thomas and King, 1974). These findings may also explain why biopsies from distal sural nerves often remain negative especially during early stages of TTR-FAP (Simmons *et al.*, 1993; Buxbaum and Tagoe, 2000; Sousa and Saraiva, 2003; Reilly, 2005; Said and Plante-Bordeneuve, 2009). In our study cohort, amyloid deposits were detectable in four of eight distal sural nerve specimens only. These biopsies were obtained from TTR-FAP patients with severe polyneuropathic symptoms, whereas the remaining four negative biopsies were obtained from patients with moderate disease. These findings further support our study results of a strong proximal to distal lesion gradient, where nerve lesions appeared predominantly at the thigh and thereby at relatively proximal levels of the peripheral nervous system. With symptom progression, nerve-lesions detected by MR-neurography were also apparent at more distal levels, correlating with the histopathological amyloid detection in more severe cases.

A hypothesis that would unify histological, clinical and imaging findings in TTR-FAP would be that endoneurial deposition and accumulation of mutant transthyretin may trigger endoneurial inflammation at a vulnerable proximal anatomical site (Sousa and Saraiva, 2003).

In summary, we were able to detect, localize and quantify nerve injury in TTR-FAP *in vivo* by MR-neurography.

Highly distinctive differences between healthy status, asymptomatic gene carriers and patients with symptomatic TTR-FAP were observed by means of (i) statistically classified MR signal alterations; (ii) microstructural parameters derived from MR signal quantification; and (iii) increase in nerve calibre. Importantly, we could show that (i) nerve injury is detectable not only in symptomatic TTR-FAP patients, but also in asymptomatic gene carriers in whom imaging detection precedes clinical and electrophysiological manifestation; and that (ii) nerve injury occurs with a strong proximal focus centred at thigh level although symptoms in TTR-FAP start and prevail distally and not proximally. High-resolution MR-neurography may become a helpful tool to detect gene carriers at risk to develop symptomatic TTR-FAP, to objectify subjective symptoms in early stages of symptomatic TTR-FAP and become particularly useful to monitor structural effects of therapeutic intervention in patients with symptomatic disease as a new and sensitive imaging biomarker. Finally, the hypothesis of proximal lesion accumulation as a trigger of length-dependent distal fibre loss is intriguing also for other distally-symmetric polyneuropathies and MR-neurography to date may be the most promising method to test this *in vivo*.

Acknowledgements

We thank Mr John M. Hayes, University of Michigan (Ann Arbor, MI, USA) for language editing and proof reading of our manuscript.

Funding

J.K. received a stipend granted from the Medical Faculty of the University of Heidelberg, and lecture honoraria as well as financial support for conference attendance from Pfizer.

E.H. received lecture honoraria and financial support for conference attendance from Pfizer. U.H. received financial support for conference attendance from Pfizer, and lecture honoraria from Celgene and Janssen. S.S. received lecture honoraria from Celgene and Janssen. J.P. received financial support for conference attendance from Pfizer. M.B. received grants and personal fees from Codman, Guerbet, Bayer and Novartis, personal fees from Roche and grants from the Hopp foundation. M.P. received a project grant from the German Osteoarthritis Foundation (Deutsche-Arthrose-Hilfe e.V.: P215-A482), a project grant from the European Foundation for the Study of Diabetes (EFSD/JDRF/Novo Nordisk European Programme in Type 1 diabetes research) and the memorial stipend from the Else-Kröner-Fresenius Foundation. The funding institutions did not have any role in study design, data collection, or analysis. The corresponding author had full access to all data and the final responsibility for the decision to submit the article for publication. All authors report no potential conflicts of interest.

References

Abbas Z, Gras V, Mollenhoff K, Keil F, Oros-Peusquens AM, Shah NJ. Analysis of proton-density bias corrections based on T measurement for robust quantification of water content in the brain at 3 Tesla. Magn Reson Med 2014; 72: 1735–45.

Adams D, Samuel D, Goulon-Goeau C, Nakazato M, Costa PM, Feray C, et al. The course and prognostic factors of familial amyloid polyneuropathy after liver transplantation. Brain 2000; 123 (Pt 7): 1495–504.

Ando Y, Coelho T, Berk JL, Cruz MW, Ericzon BG, Ikeda S, et al. Guideline of transthyretin-related hereditary amyloidosis for clinicians. Orphanet J Rare Dis 2013; 20: 8–31.

Andrade C. A peculiar form of peripheral neuropathy; familiar atypical generalized amyloidosis with special involvement of the peripheral nerves. Brain 1952; 75: 408–27.

Bendszus M, Stoll G. Technology insight: visualizing peripheral nerve injury using MRI. Nat Clin Pract Neurol 2005; 1: 45–53.

Benson MD. Familial amyloidotic polyneuropathy. Trends Neurosci 1989; 12: 88–92.

Benson M. Amyloidosis. In: Scriver CR, Sly WS, Valle D, editors. The metabolic and molecular basis of inherited disease. New York: McGraw-Hill; 1995. p. 4159–91.

Bergethon PR, SabinTD , Lewis D, Simms RW, Cohen AS, Skinner M. Improvement in the polyneuropathy associated with familial amyloid polyneuropathy after liver transplantation. Neurology 1996; 47: 944–51.

Berk JL, Suhr OB, Obici L, Sekijima Y, Zeldenrust SR, Yamashita T, Heneghan MA, et al. Repurposing diflunisal for familial amyloid polyneuropathy: a randomized clinical trial. JAMA 2013; 310: 2658–67.

Bril V. NIS-LL: the primary measurement scale for clinical trial endpoints in diabetic peripheral neuropathy. Eur Neurol 1999; 41 (Suppl 1): 8–13.

Buxbaum JN, Tagoe CE. The genetics of the amyloidoses. Annu Rev Med 2000; 51: 543–69.

Coelho T, Maia LF, Martins da Silva A, Waddington Cruz M, Plante-Bordeneuve V, Lozeron P, et al. Tafamidis for transthyretin familial amyloid polyneuropathy: a randomized, controlled trial. Neurology 2012; 79: 785–92.

Coelho T, Adams D, Silva A, Lozeron P, Hawkins PN, Mant T, et al. Safety and efficacy of RNAi therapy for transthyretin amyloidosis. N Engl J Med 2013; 369: 819–29.

Coutinho P, Martins Da Silva A, Lopes Lima J, Resende Barbosa A. Forty years of experience with type I amyloid neuropathy: review in 483 cases. In: Glenner GG, Pinho P, Costa E, Falcao De Freitas A, editors. Amyloid and amyloidosis. Amsterdam: Excerpta Medica; 1980. p. 88.

Davies GR, Ramani A, Dalton CM, Tozer DJ, Wheeler-Kingshott CA, Barker GJ, et al. Preliminary magnetic resonance study of the macromolecular proton fraction in white matter: a potential marker of myelin? Mult Scler 2003; 9: 246–9.

De Navasquez S, Treble HA. A case of primary generalized amyloid disease with involvement of the nerves. Brain 1938; 61: 116–28.

Dyck PJ, Lambert EH. Dissociated sensation in amyloidosis: compound action potentials; quantitative histologic and teased fibers; and electron microscopic studies of sural nerve biopsies. Trans Am Neurol Assoc 1968; 93: 112–5.

Dyck PJ, Karnes JL, O'Brien P, Okazaki H, Lais A, Engelstad J. The spatial distribution of fiber loss in diabetic polyneuropathy suggests ischemia. Ann Neurol 1986a; 19: 440–9.

Dyck PJ, Lais A, Karnes JL, O'Brien P, Rizza R. Fiber loss is primary and multifocal in sural nerves in diabetic polyneuropathy. Ann Neurol 1986b; 19: 425–39.

Dyck PJ. Detection, characterization, and staging of polyneuropathy: assessed in diabetics. Muscle Nerve 1988; 11: 21–32.

Dyck PJ, Davies JL, Litchy WJ, O'Brien PC. Longitudinal assessment of diabetic polyneuropathy using a composite score in the Rochester Diabetic Neuropathy Study cohort. Neurology 1997; 49: 229–39.

Dyck PJ, Norell JE. Microvasculitis and ischemia in diabetic lumbosacral radiculoplexus neuropathy. Neurology 1999; 53: 2113–21.

Enderlein G. Scheffé, H.: The analysis of variance. Wiley, New York 1959. Biom J 1961; 3: 143–4.

Filler AG, Howe FA, Hayes CE, Kliot M, Winn HR, Bell BA, et al. Magnetic resonance neurography. Lancet 1993; 341: 659–61.

Gioeva Z, Urban P, Meliss RR, Haag J, Axmann HD, Siebert F, et al. ATTR amyloid in the carpal tunnel ligament is frequently of wild-type transthyretin origin. Amyloid 2013; 20: 1–6.

Hanyu N, Ikeda S, Nakadai A, Yanagisawa N, Powell HC. Peripheral nerve pathological findings in familial amyloid polyneuropathy: a correlative study of proximal sciatic nerve and sural nerve lesions. Ann Neurol 1989; 25: 340–50.

Heiland S, Sartor K, Martin E, Bardenheuer HJ, Plaschke K. *In vivo* monitoring of age-related changes in rat brain using quantitative diffusion magnetic resonance imaging and magnetic resonance relaxometry. Neurosci Lett 2002; 334: 157–60.

Holmgren G, Ericzon BG, Groth CG, Steen L, Suhr O, Andersen O, et al. Clinical improvement and amyloid regression after liver transplantation in hereditary transthyretin amyloidosis. Lancet 1993; 341: 1113–6.

Holmgren G, Steen L, Ekstedt J, Groth CG, Ericzon BG, Eriksson S, et al. Biochemical effect of liver transplantation in two Swedish patients with familial amyloidotic polyneuropathy (FAP-met30). Clin Genet 1991; 40: 242–6.

Hund E, Linke RP, Willig F, Grau A. Transthyretin-associated neuropathic amyloidosis. Pathogenesis and treatment. Neurology 2001; 56: 431–5.

Hund E. Familial amyloidotic polyneuropathy: current and emerging treatment options for transthyretin-mediated amyloidosis. Appl Clin Genet 2012; 5: 37–41.

Jenkinson M, Beckmann CF, Behrens TE, Woolrich MW, Smith SM. Fsl. Neuroimage 2012; 62: 782–90.

Johnson SM, Connelly S, Fearns C, Powers ET, Kelly JW. The transthyretin amyloidoses: from delineating the molecular mechanism of aggregation linked to pathology to a regulatory-agency-approved drug. J Mol Biol 2012; 421: 185–203.

Kebbel A, Rocken C. Immunohistochemical classification of amyloid in surgical pathology revisited. Am J Surg Pathol 2006; 30: 673–83.

Kelly JJ Jr, Kyle RA, O'Brien PC, Dyck PJ. The natural history of peripheral neuropathy in primary systemic amyloidosis. Ann Neurol 1979; 6: 1–7.

Kollmer J, Baumer P, Milford D, Dombert T, Staub F, Bendszus M, et al. T2-signal of ulnar nerve branches at the wrist in guyon's canal syndrome. PLoS One 2012; 7: e47295.

Merlini G, Plante-Bordeneuve V, Judge DP, Schmidt H, Obici L, Perlini S, et al. Effects of tafamidis on transthyretin stabilization and clinical outcomes in patients with non-Val30Met transthyretin amyloidosis. J Cardiovasc Transl Res 2013; 6: 1011–20.

Pham M, Oikonomou D, Baumer P, Bierhaus A, Heiland S, Humpert PM, Nawroth PP, et al. Proximal neuropathic lesions in distal symmetric diabetic polyneuropathy: findings of high-resolution magnetic resonance neurography. Diabetes Care 2011; 34: 721–3.

Pham M, Baumer P, Meinck HM, Schiefer J, Weiler M, Bendszus M, et al. Anterior interosseous nerve syndrome: fascicular motor lesions of median nerve trunk. Neurology 2014; 82: 598–606.

Plante-Bordeneuve V, Lalu T, Misrahi M, Reilly MM, Adams D, Lacroix C, et al. Genotypic-phenotypic variations in a series of 65 patients with familial amyloid polyneuropathy. Neurology 1998; 51: 708–14.

Plante-Bordeneuve V, Said G. Familial amyloid polyneuropathy. Lancet Neurol 2011; 10: 1086–97.

Rajani B, Rajani V, Prayson RA. Peripheral nerve amyloidosis in sural nerve biopsies: a clinicopathologic analysis of 13 cases. Arch Pathol Lab Med 2000; 124: 114–118.

Reilly M. Hereditary amyloid neuropathy. In: Dyck PJ, editor. Peripheral neuropathy. Vol. 2. Elsevier Saunders: Philadelphia; 2005. p. 1921–35.

Said G, Ropert A, Faux N. Length-dependent degeneration of fibers in Portuguese amyloid polyneuropathy: a clinicopathologic study. Neurology 1984; 34: 1025–32.

Said G, Plante-Bordeneuve V. Familial amyloid polyneuropathy: a clinico-pathologic study. J Neurol Sci 2009; 284: 149–54.

Said G, Plante-Bordeneuve V. TTR-familial amyloid polyneuropathy–neurological aspects. Amyloid 2012; 19 (Suppl 1): 25–7.

Schonland SO, Hegenbart U, Bochtler T, Mangatter A, Hansberg M, Ho AD, et al. Immunohistochemistry in the classification of systemic forms of amyloidosis: a systematic investigation of 117 patients. Blood 2012; 119: 488–93.

Shahani BT, Halperin JJ, Boulu P, Cohen J. Sympathetic skin response–a method of assessing unmyelinated axon dysfunction in peripheral neuropathies. J Neurol Neurosurg Psychiatry 1984; 47: 536–42.

Shivji ZM, Ashby P. Sympathetic skin responses in hereditary sensory and autonomic neuropathy and familial amyloid neuropathy are different. Muscle Nerve 1999; 22: 1283–6.

Simmons Z, Blaivas M, Aguilera AJ, Feldman EL, Bromberg MB, Towfighi J. Low diagnostic yield of sural nerve biopsy in patients with peripheral neuropathy and primary amyloidosis. J Neurol Sci 1993; 120: 60–3.

Sousa MM, Saraiva MJ. Neurodegeneration in familial amyloid polyneuropathy: from pathology to molecular signaling. Prog Neurobiol 2003; 71: 385–400.

Stoll G, Bendszus M. Imaging of inflammation in the peripheral and central nervous system by magnetic resonance imaging. Neuroscience 2009; 158: 1151–60.

Stoll G, Bendszus M, Perez J, Pham M. Magnetic resonance imaging of the peripheral nervous system. J Neurol 2009; 256: 1043–51.

Sugimura K, Dyck PJ. Multifocal fiber loss in proximal sciatic nerve in symmetric distal diabetic neuropathy. J Neurol Sci 1982; 53: 501–9.

Thomas PK, King RH. Peripheral nerve changes in amyloid neuropathy. Brain 1974; 97: 395–406.

Tofts PS, du Boulay EP. Towards quantitative measurements of relaxation times and other parameters in the brain. Neuroradiology 1990; 32: 407–15.

Tojo K, Sekijima Y, Kelly JW, Ikeda S. Diflunisal stabilizes familial amyloid polyneuropathy-associated transthyretin variant tetramers in serum against dissociation required for amyloidogenesis. Neurosci Res 2006; 56: 441–9.

Van Allen MW, Frohlich JA, Davis JR. Inherited predisposition to generalized amyloidosis. Clinical and pathological study of a family with neuropathy, nephropathy, and peptic ulcer. Neurology 1969; 19: 10–25.

Yumlu S, Barany R, Eriksson M, Rocken C. Localized insulin-derived amyloidosis in patients with diabetes mellitus: a case report. Hum Pathol 2009; 40: 1655–60.